LA-10619-HDR, Part 1

UC-66b
Issued: July 1987

LA--10619-HDR-Pt.1

DE87 014710

Geological Structures from Televiewer Logs of GT-2, Fenton Hill, New Mexico

Part 1: Feature Extraction

Kerry L. Burns

Los Alamos National Laboratory
Los Alamos, New Mexico 87545

DISCLAIMER

CONTENTS

GEOLOGICAL STRUCTURES FROM TELEVIEWER LOGS OF GT-2, FENTON HILL, NEW MEXICO

Part 1: Feature Extraction

by

Kerry L. Burns

ABSTRACT

Patterns in reflected sonic intensity recognized during examination of televiewer logs of basement gneiss at the Hot Dry Rock Site, Fenton Hill, New Mexico, are due to geological fractures and foliations and to incipient breakouts. These features are obscured by artifacts caused by wellbore ellipticity, tool off-centering, and tool oscillations. An interactive method, developed for extraction of the structural features (fractures and foliations), uses human perception as a pattern detector and a chi-square test of harmonic form as a pattern discriminator. From imagery of GT-2, 733 structures were recovered. The acceptance rate of the discriminator was 54%. Despite these positive results, the general conclusion of this study is that intensity-mode imagery from Fenton Hill is not directly invertible for geological information because of the complexity of the televiewer imaging process. Developing a forward model of the intensity-imaging process, or converting to caliper-mode imagery, or doing both will be necessary for high-fidelity feature extraction from televiewer data.

I. INTRODUCTION

A. Scope of This Report

We have developed a method of extracting structural data from televiewer imagery using as trial data some extremely poor imagery from GT-2 at Fenton Hill. This report describes some of the features that have been recognized and a simple method of pattern discrimination for geological structures.

Questions addressed in this report are (1) what features in the rock or on the wellbore surface can be detected with a televiewer? (2) what is the physical process that enables them to be detected? and (3) how may the instrument or data processing be modified to improve detectability? Two specific questions are (4) how could the aperture of fractures be measured with this instrument? and (5) is the observed diffuse texture, interpreted as foliation, due to resolution of discrete laminae or to a diffraction effect from a field of unresolved objects?

Technical terms that require some explanation are shown in caps at their first appearance, for example, DETECTABILITY.

B. The Hot Dry Rock Geothermal Energy Program

Drill hole GT-2 (Geothermal Test well No. 2) was drilled in 1974 to a total depth of 2932 m (9619 ft) at the Fenton Hill geothermal site in the Jemez Mountains of northern New Mexico (Pettitt 1975c). The upper 0.73 km was in a cover of volcanics and sediments and the remaining 2.27 km in a basement of Precambrian metamorphics, predominantly hornblende-biotite granite gneiss. This borehole, along with its neighbor EE-1 (Energy Extraction hole No. 1), was used, in 1975-1980, to prove the scientific feasibility of extracting energy from hydraulically fractured rock. This research program, the Hot Dry Rock Program, is currently continuing with two hotter and deeper wells.

C. Geological Environment of GT-2

Descriptions of the geological environment include the geology (Purtymun 1973; Purtymun et al. 1974; Kintzinger and West 1976; Kintzinger et al. 1978); petrology (Perkins 1973); geohydrology (West 1974); and seismicity (Slemmons 1975).

D. Previous Studies of GT-2

Descriptions of GT-2 include drilling operations (Pettitt 1975a,b,c); temperature (Albright 1975); hydrology (West et al. 1975a); geophysical logs (West et al. 1975b; West and Laughlin 1976); geology (Purtymun et al. 1974); petrology (Heimlich 1976; Laughlin and Eddy 1977; Laughlin et al. 1983); isotope geochemistry (Brookins et al. 1977; Zartment 1979; Brookins and Laughlin 1983); microcracks (Simmons and Eddy 1976); permeability (Delisle 1975; Trice and Warren 1977); in situ stress (Aamodt 1974, 1977); and thermal conductivity (Sibbitt 1976). However, descriptions of macroscopic structure are limited to observations of recovered core, and the televiewer remains the best hope for measuring rock-mass properties in situ.

II. THE TELEVIEWER INFORMATION-GATHERING SYSTEM

A. Downhole Viewing Instruments

Three different instruments are used for inspection of boreholes. The STRATASCOPE is an optical periscope that is inserted into a drill hole and used to look for "splits" or "partings" between stratifications intersected by the well (East and Gardner 1964). The BOREHOLE CAMERA is an optical wide-angle camera that intermittently takes pictures downhole. Four different types of cameras are described by Dempsey and Hickey (1958), Jensen and Ray (1965), Mullins (1966), and Kotyakhov and Serbrennikov (1964). An example of borehole camera images is shown in Zemanek et al. (1970, Figure 5, p. 259). The BOREHOLE TV is an optical wide-angle video camera that returns an image to a television screen at the surface. One type, described by Briggs (1964), is used to inspect the condition of overburden and mine openings in coal mine subsidence control work. The TELEVIEWER is a sonic scanner that scans the wellbore and returns electronic imaging data, line by line, to a surface recorder, as described by Zemanek et al. (1969, 1970) and Hinz and Schepers (1981). The televiewer is a borehole scanner and is similar to aircraft and satellite scanners.

B. Information Flow

The televiewer information-gathering system comprises three subsystems: data acquisition, feature extraction, and geological or geotechnical interpretation. DATA ACQUISITION comprises instrument design, operation, recording, and playback. FEATURE EXTRACTION is extraction of geological or geotechnical features from the played-back recording or from reconstructed images. INTERPRETATION is interpretation of extracted features for parameters of geological or geotechnical significance. This report is concerned with feature extraction.

III. TELEVIEWER DATA ACQUISITION

A. Field Operations in GT-2

The USGS first conducted televiewer surveys of GT-2 between depths of 3270-3350 ft and 3445-3590 ft in mid 1974. These surveys were not oriented because the magnetometer failed to operate at temperatures in the hole (Pettitt 1975a). The present logs, supplied by Bob Potter of LANL, were run

by Scott Keys of the USGS in December 1974. They are not mentioned in Pettitt (1975b,c).

B. Description of Instrument

A schematic drawing of a borehole televiewer is given in Figure 1. The USGS televiewer consisted of a piezoelectric transducer, rotating right-handedly, that converted reflected sonic intensity to electrical signals. The signals were brought uphole and were used to drive the intensity of a cathode ray oscilloscope. The CRT sweep was triggered by a magnetometer when the sensor crossed the magnetic meridian. The CRT trace height was advanced by

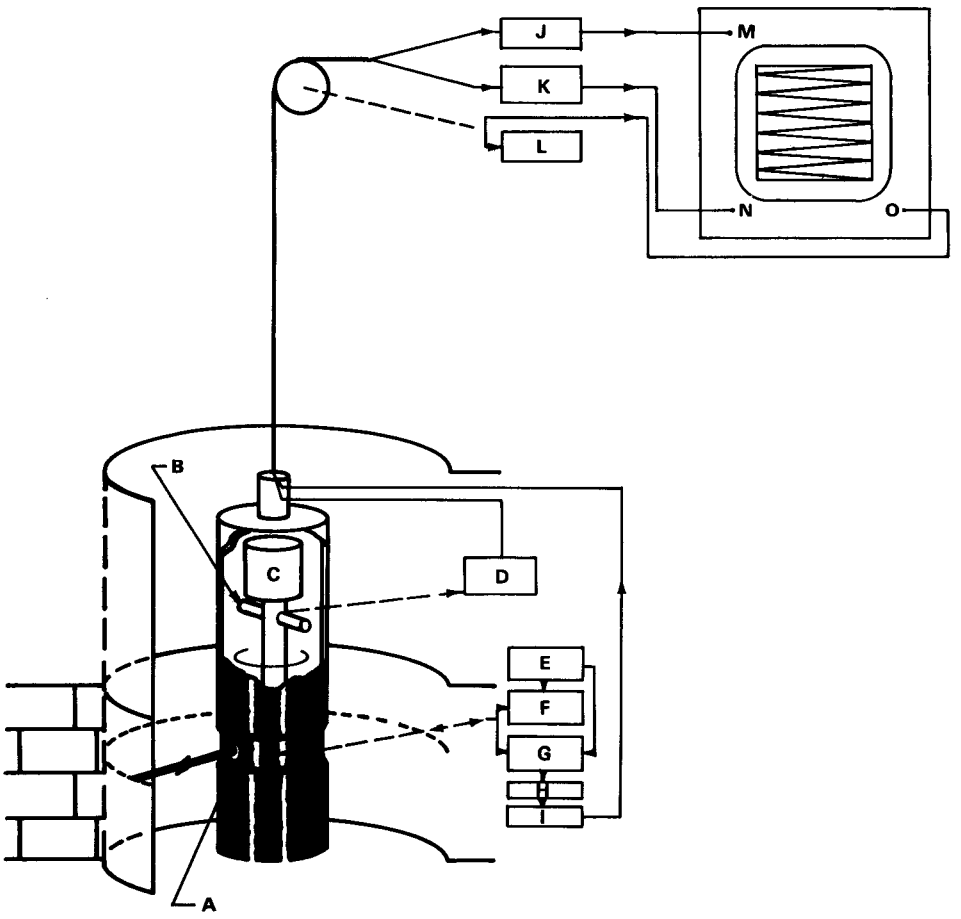

Figure 1. Schematic diagram of the original borehole televiewer. Symbols for downhole hardware are A. piezoelectric transducer, B. fluxgate magnetometer, and C. drive motor. Symbols for downhole electronics are D. orientation pulse generator, E. 2000-Hz oscillator, F. transmitter pulse generator, G. signal gate, H. amplifier, and I. detector. Symbols for uphole electronics are J. amplifier, K. sweep generator, L. depth potentiometer. The oscilloscope controls are M. Z-axis, N. horizontal sweep, and O. vertical sweep. Modified from Zemanek et al. 1969, Figure 1, p.763.

one scan line for each rotation of the sensor. The CRT image was recorded with a Polaroid instant camera. Each image covered an azimuth range of 360° and a nominal depth range of 20 ft. Televiewers have two modes of operation. In the INTENSITY MODE, the instrument measures intensity of the reflected pulse and writes an image to film in which the film density indicates received intensity, depending upon the film response characteristics. In CALIPER MODE, the instrument measures flight time of the sonic pulse in traveling to the wellbore and back so that an image reconstructed from this data portrays the geometry of the wellbore. The USGS records of GT-2 are in intensity mode.

C. Instrumental Parameters

Piezoelectric transducers with a 1.3-MHz frequency are used. The velocity of sound at a depth of 3000 m in brine at 0°C is 1500 m/s (Forsythe 1954, Table 299, p. 307). By the linear approximation of Howell (1959, p. 182), this velocity may be extrapolated to 2076 m/s at 250°C. The wavelength is then 1.6 mm. The propagation constant, K, defined as 2π/wavelength, is 3.9 cycles/mm.

The wellbore is nominally a circular cylinder. In the plane normal to the wellbore axis, the wellbore surface resembles a rough, concave mirror. Rays emitted by the transducer are brought back into focus at the center of the transducer at the center of the wellbore. The radius of the concavity ranges from the nominal wellbore diameter, 9-5/8 in., to about 13-1/4 in., or from 244 to 377 mm. A return pulse can be identified and the time of flight measured accurately to a distance of 0.2 mm.

In diameter (D) the face of the transducer is about 3/4 in. and is about 1 in. from the center of the wellbore. The beam spreads in traveling from the face of the transducer to the wellbore. A rule of thumb is that the beam doubles in width in a distance kD, where k is the number of wavelengths in D. This rule yields a spreading angle of about 5° for this instrument. The transducer then subtends an arc length of about 8 mm at the wellbore. The INSTANTANEOUS FIELD OF VIEW (or IFOV) has a radius of 4 mm at the wellbore. Other properties of a cyclindrical piezoelectric transducer are described by Zemanek (1971).

The transducer rotates at 3 rps, so at a logging speed of 20 ft/min, the ALONG-TRACK or SCAN-LINE spacing on the wellbore is 9 scan lines/ft or 34 mm. At 5 ft/min logging speed, the along-track spacing is 8.5 mm. The transducer is fired at 128 shots/revolution that, for a 9-5/8-in.-diam wellbore, is a

CROSS-TRACK or SHOT spacing of 6 mm. The IFOVs for two adjacent shots have a linear overlap of 62%, which means that two successive shots are quite well correlated.

The televiewer output for GT-2 was written to a CRT with the vertical ramp set so that two adjacent scan lines had about 10% SIDELAP, and the CRT display was then recorded with an instant camera. The resulting frames had a scan-line length of 60 mm, recording a cross-track rotation through 360° and a frame height of 57 mm, recording 20 ft of wellbore depth along-track. The spacings were about 2 shots/mm across-track and, at a logging speed of 20 ft/min, about 3 lines/mm along-track. At a logging speed of 5 ft/min, the along-track spacing was about 12 lines/mm. The PIXEL or PICTURE ELEMENT, which was introduced by Schade (1948b) as the spot on the image corresponding to the IFOV on the object, was 0.5 mm across-track and from 0.1 to 0.3 mm along-track.

IV. FEATURE DETECTION

A. Intensity and Density

The term INTENSITY applied to a waveform is the usual product of complex amplitude with its conjugate value (Joos 1958, p. 724). When a film is exposed, the exposure E is the product of intensity by time. The resultant film DENSITY, D, is a nonlinear function of E termed the characteristic curve of the film. This usually has a RAMP portion in which D = G*LN(E) + H (Campbell 1962), where G and H are constants for the film, G being the film GAMMA and LN the usual Naperian logarithm. The density of a televiewer image is therefore a function of detected return intensity, CRT phosphor characteristics, and film response (Schade 1964).

B. Detectability, Measurability, and Visibility

The term resolution is defined in terms of the Rayleigh criterion (Waters 1981, p. 270), which gives the minimum angular separation for distant, high-contrast point objects. For nontelescopic systems the Rayleigh spread function is not the only obscuring mechanism, and a variety of different measures have been developed. After Welch (1972), we use the terms DETECTABILITY, meaning the ability to determine whether a known object can be detected or not,

and MEASURABILITY, the ability to make measurements of size and other properties, such as the aperture of fractures, from objects detected on the imagery. VISIBILITY is used to mean both detectability and measurability (Duntley 1948; Schade 1948a).

Schade (1948a,b, 1964) examined visibility of rectangular bar targets in television. Detection required a minimum contrast between bar and background of 1.8:1. The number of TV lines required to detect high-contrast (1000:1) and low-contast (1.6:1) targets is 2.8 and 4, respectively. In satellite remote sensing, the multispectral scanner system (MSS) has a 79-m IFOV and a 56-m cross-track interval at the object. Colvocoresses (1972) used Schade's TV criteria to predict resolutions of 136 m and 180 m for high- and low-contrast targets, respectively. Bachofer (1973) and Haas et al. (1972) used a different method to estimate about 70 m for medium-contrast targets and verified that estimate from imagery. Rosenberg (1971) explained the different results as a difference between resolution and detectability. NASA (1972, p. F-22) said the theoretical limit of detectability was 1/2 IFOV.

C. Structures, Features, and Artifacts

Geological features are induced physically real objects on the surface of the wellbore such as vughs, chips, breakouts, and geological structures. Geological structures are natural or induced joints, faults, cleavages, foliations, and bedding. Structures observed on GT-2 include fractures and gneissic foliation, the latter comprising discrete bands and folia as well as diffuse foliations such as preferred orientation. Another natural feature on GT-2 is chipping or spalling on the trace of discrete structures such as joints or thin micaceous folia. The chips are possibly incipient breakouts.

Artifacts are features on the imagery that do not correspond to physically real objects on the wellbore. Televiewer imagery has recording artifacts in common with return beam vidicon (RBV) imagery (Clark 1981) and geometric artifacts in common with MSSs on satellite or aircraft platforms (Masry and Gibbon 1973). Recording artifacts include repetition and omission of scan lines and line dropouts between frames. Geometric distortions include distortion, harmonic shading, and oscillation patterns such as striae, striping, and grain effect.

The term SYSTEM ABERRATIONS is used for astigmatism due to differential curvature of the wellbore (see, for example, Joos 1958, p. 408) and spherical

aberration due to an elliptical wellbore (see, for example, Caunt 1914, exercise 30, p. 421) or an off-centered tool.

Selections of imagery showing various structures and other natural features and artifacts are shown in Figures 2-9. These images cover 40 ft in depth, ranging from top to bottom as marked and 360° in azimuth, ranging from 0° to 360° east of magnetic north from left to right.

D. Fractures

Joints and fractures are open to the wellbore or filled with soft materials such as calcite and chlorite. Their apertures probably range from hairline cracks to cracks of several millimeters. Conspicuous examples are shown in Figures 2, 3, 7, and 8.

The characteristic texture associated with fractures on intensity-mode imagery is a dark, discrete linear feature: first, the reflected intensity at a pixel is reduced below that at neighboring pixels; and second, the pixels with reduced intensity are placed on neighboring scan lines so that they are adjacent at a side or edge. We define CONNECTIVITY of a pixel in a feature as the number of neighboring pixels that are also in the feature. Then the textural feature can be defined as a connected object with connectivity of one. Fractures are visible at a fraction of the IFOV, a dimension that is substantially below NASA's theoretical limit. The reason for this anomalous result is probably absorption.

The process causing absorption by fractures is probably the "razor-blade" or wave-guide effect of Weisskopf (1968). Fractures are apertures that continue into the rock. Rays entering an aperture are dissipated by reflection and scattering from the sides so that this part of the IFOV is subtracted from the reflected intensity. If the aperture is less than one wavelength, or about 2 mm, diffraction over the aperture, as illustrated by Sheriff and Geldart (1982, Figure 4.25, p. 121), would reduce the absorbent effect.

The effect of absorption at a pixel containing a fracture, in ratio to neighboring pixels not containing a fracture, may be estimated as I(F,G,W,R,A):

$$I = [2FRW + G(A - 2RW)]/(GA), \qquad (1)$$

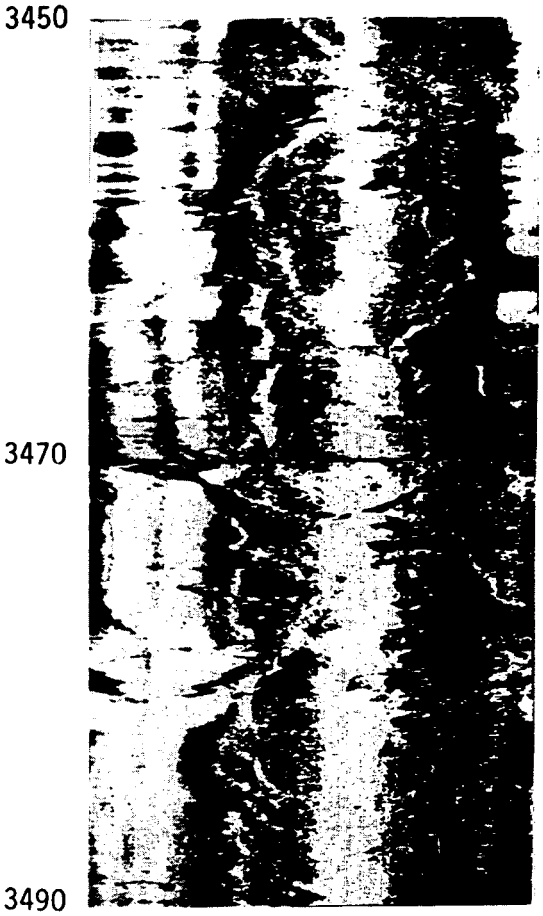

Figure 2. Image from 3450 to 3490 ft depth. Two fractures appear as sinusoidal traces at about 3475 and 3480 ft. The two straight, vertical, wide, bright stripes are harmonic shading. The vertical bright pattern of disconnected triangular patches may be due to breakouts.

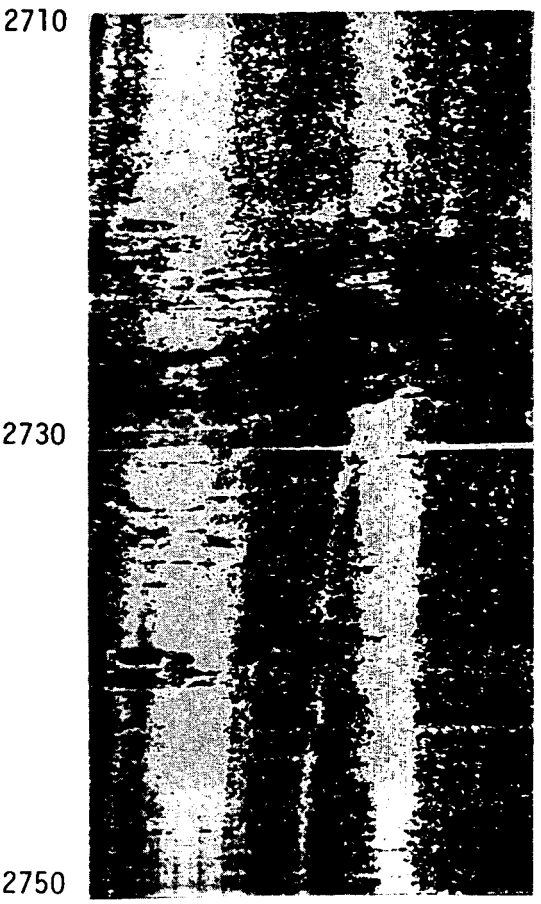

Figure 3. Image from 2710 to 2750 ft depth. A wide fracture appears as a sinusoidal trace at about 2725 ft. The close-spaced discontinuous traces immediately above and below the fracture may be foliation at an angle to the fracture.

Figure 4. Image from 4500 to 4540 ft depth. The close-spaced discontinuous traces between about 4525 and 4530 ft are probably foliation.

Figure 5. Image from 4210 to 4250 ft depth. A band in the foliation from about 4212 to 4216 ft shows as a region of distinctive textural statistics.

Figure 6. Image from 6320 to 6360 ft depth. The artifact from about 6342 to 6360 ft is due to the tool moving with a nonrotating transducer. This is at the start of a run. Between about 6320 and 6342 ft, the linear patches sloping downward to the right are a grain effect, possibly due to oscillations as the tool accelerates. The dark horizontal lines in a bundle at about 6335 ft are scan-line dropouts.

Figure 7. Image from 3830 to 3870 ft depth. The irregular dark line at 3850 ft is a steeply dipping fracture. The triangular black patch at 3852 ft is an incipient breakout.

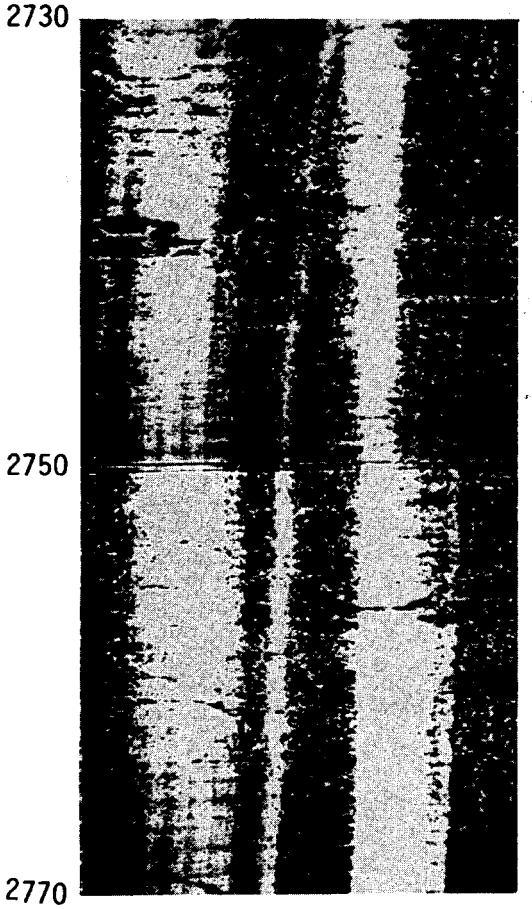

Figure 8. Image from 2730 to 2770 ft depth. The two straight, vertical, wide, bright stripes are harmonic shading. The steep, gently curving, narrow bright lines are striations. The harmonic shading may be rectilinear due to the wellbore being a quadric cylinder, with the stripes being generators of the cylinder.

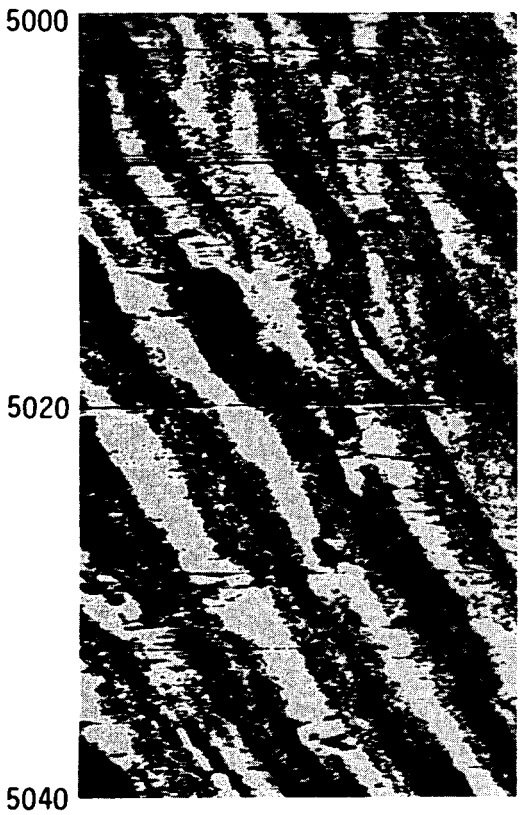

Figure 9. Image from 5000 to 5040 ft depth. The artifacts appear to be the same as for Figure 7. The obliquity may be due to the wellbore being rifled, the tool being badly off-centered, or failure of the magnetometer trigger.

where A is the area of the IFOV, R is the radius of the IFOV (4 mm in this case), W is the width of the fracture, and F/G is the ratio of coefficients of reflection for the fracture and country rock, respectively. If intensity is reduced by a proportion P, then $I = 1 - P$. A reduction in reflected intensity to $P = 0.1$ yields W of about 0.6 mm, which would be, approximately, the smallest detectable aperture.

Measurability is different from detectability, and apertures below the IFOV are unmeasurable by metrication on intensity-mode imagery. Possibly they could be measured if the reflected intensity were known, if the coefficients of reflection were known, and if a model or numerical simulation were available to evaluate particulars such as the diffraction and wave-guide effects for specified joint apertures, joint attitudes, hole caliper, tool position in the hole, sonic velocity in the borehole fluid, and transducer characteristics.

E. Foliation in Gneiss

Foliation is due to several different mineralogical objects having a wide range of sizes. Here we classify them into three size ranges. The smallest is a mineral GRAIN, ranging from 0.3 to 5 mm in diameter. The next size is a discrete mineral FOLIUM, or layer of minerals, ranging in thickness from about 5 to about 30 mm. The largest size is a discrete mineral BAND, such as a felsic layer, ranging in size from about 20 mm to about 6 m. Spacing of foliations along a line is more complex than spacing for joints because the foliations are selected at random from, at least, these three different size distributions and because they are nested; that is, a band may be foliated and a folium is always grainy. Mean spacings of 3 mm for grains, 10 mm for folia, and 30 mm for bands were estimated from hand specimens of gneiss similar to that at Fenton Hill, from the Santa Fe ski basin (Figure 10).

The foliation at a coarse scale (folia and bands) comprises DISCRETE mineralogical objects because a decision criterion can be found based upon proportions of quartz, feldspar, and mica, which would partition the rock into finite, bounded, connected objects. However, the foliation at a fine scale (grain scale) is a preferred orientation, as defined by Turner and Weiss (1963, p. 394), and is determined by grain shape. It is a DIFFUSE foliation or mineralogical pattern parameter. The spatial, two-dimensional Fourier transform (as described by Davis and Preston 1972; Preston and Davis 1972) of

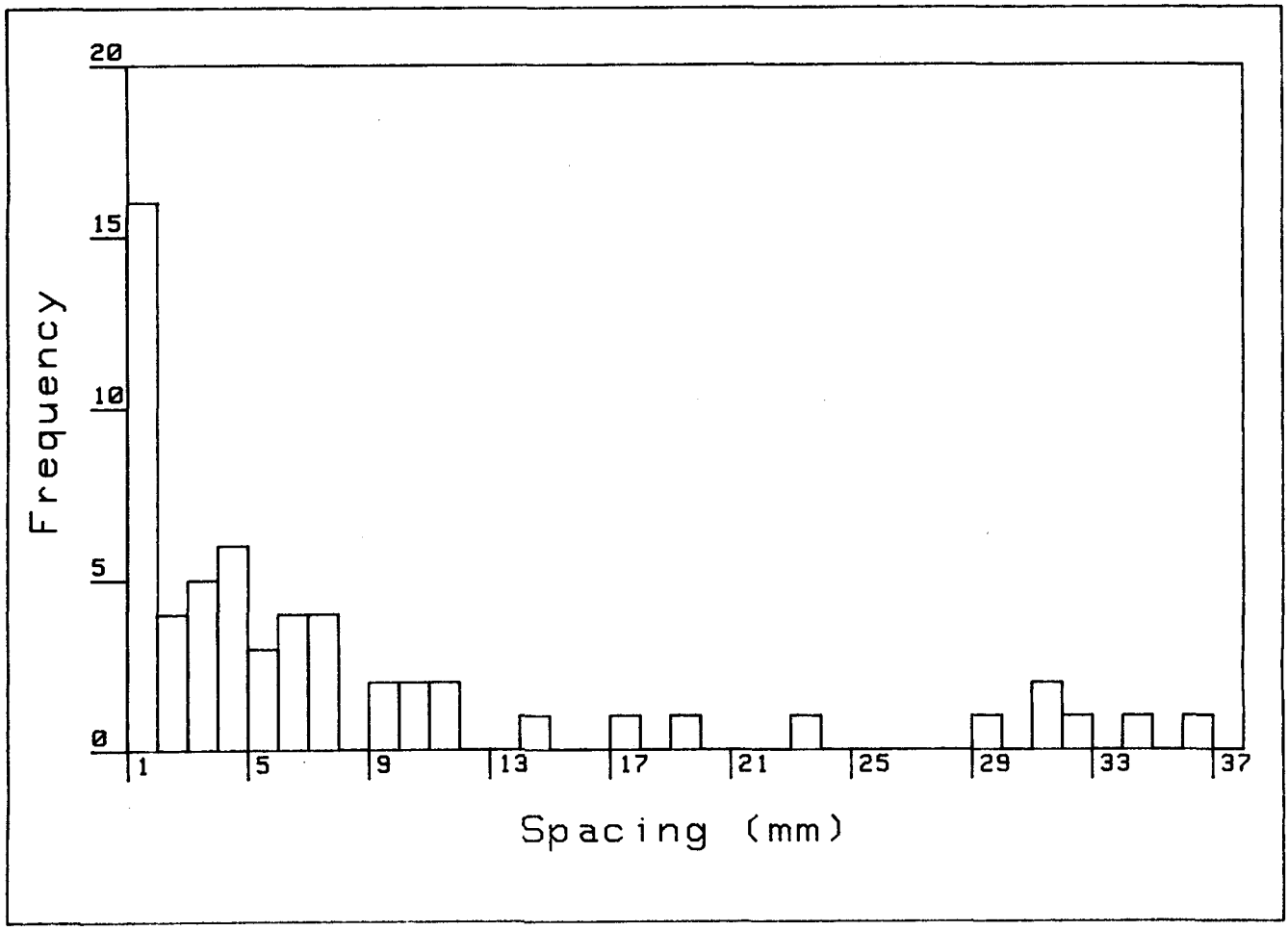

Figure 10. Spacing of foliations in hand specimen of gneiss.

both gneisses and sedimentary rocks is different for high and low spatial frequencies. The low-frequency objects are distinct folia and bands, with a flat (DC) spectrum in one direction, with dominant spatial frequencies in two perpendicular directions in the ratio 0.1:0 or 0.03:0 mm^{-1}. The high-frequency objects are fields of elongated grains, with a ratio of about 0.3:0.2 mm^{-1}.

F. Discrete Foliation

The coefficient of reflectance varies between adjacent folia. The amplitude of a secondary wave (reflection or diffraction) is proportional to the intensity of the incident wave and to the size, density, and bulk modulus of the target minerals (Waters 1981, p. 292). The most important difference is probably in bulk modulus between feldspar, mica, and quartz; representative ratios are 1.55:1.18:1 (Forsythe 1954, Table 840, p. 740). This would make

foliation a low-contrast target on Schade's criteria. The close-spaced, parallel, thin layers above and below the fracture in Figure 3 may be discrete folia.

1. Mineral Bands. Bands are expressed as regions of different first- and second-order textural statistics (as defined by Julesz 1975). An example is shown in Figure 5.

2. Folia. Discrete linear objects that are not fractures are both bright and dark. When we use Equation (1) with the same density threshold, P, of 0.1 but with the low reflectance contrast F:G of 1:1.5, the minimum detectable width is 3.5 mm. Grains of this width are not long enough to continue over several adjacent scan lines, so the only objects detected in this way are thin, prolonged mica folia (dark) or thin felsitic veins (bright). They have been identified on GT-2 imagery by the diffuse textural features attributed to foliation that parallel both of them. An example is shown in Figure 4. Without this confirmation, thin, dark micaceous folia cannot be distinguished from fractures. The identification is confirmed on GT-2 by a correspondence between some felsite veins (light) and peaks on gamma-ray logs and between some dark veins and peaks on caliper logs. In this case, the image features correspond to real objects, and the IFOV grid is acting as a low-pass filter.

G. Diffuse Foliation

Diffuse structures appear on imagery as fields of fine striae of high spatial frequency, which are detected by their obliquity and consistent parallelism over depths of more than 5 ft. The textural statistics of the diffuse texture have not been quantified. Texture can be described as a pattern of parallel bright linears of high spatial frequency. Examples are shown in Figures 3, 4, and 5.

Preferred orientations are fields of elongated grains, with a ratio of spatial frequencies in two perpendicular directions of about 0.3:0.2 mm^{-1}. The diffuse foliation might be an eigenfeature of this texture.

Mechanisms by which this structure becomes visible are unknown. Possibilities include spurious resolution (Hotchkiss et al. 1950, 1951), edge diffraction (Keller 1961; Trorey 1970), a phase grating (McLaren et al. 1970), and Mach banding (Morrone et al. 1986). Not knowing the specific mechanisms responsible for the diffuse texture, we cannot know whether the correspondence between geological objects on the wellbore and textural features on the image is one-to-one or many-to-one, that is, whether the features are real objects

or rainbows. For example, Morrone et al. (1986) describe Mach bands as "paradoxical bands of light and dark" due to "lateral inhibition in the visual system."

Diffuse foliation is found on USGS intensity-mode imagery from GT-2 and EE-3A. However, intensity-mode imagery made with other instruments had not shown the diffuse foliation, perhaps because texture may be easily destroyed by electronic recording processes such as automatic gain control or by routine image-enhancement processes such as scan-line equalization.

H. Breakouts

Fractures and thin, dark micaceous seams frequently have small triangular wedges at intervals along their trace. An example is shown in Figure 7. These chips or spalls may be chattermark due to tool abrasion or, more likely, incipient breakouts of the type reported by Plumb and Hickman (1985).

I. Harmonic Shading

Shading, a tonal gradation described by Clarke (1981), is pronounced on the televiewer imagery of GT-2. Examples are shown in Figures 2, 3, 4, 6, 7, and 8. The effect is vertical banding of the images into alternating over- and underexposed strips. In many places, the shading is rectilinear, that is, in straight strips running parallel or at low angle to the axis of the wellbore. The film density varies across-track as a harmonic function of azimuth, namely COS(2*Azimuth), hence the name "harmonic" shading. The major cause of harmonic shading is probably noncircularity of the wellbore and off-centering of the tool. The angle of incidence of the sonic ray with the wellbore surface changes with azimuth in such a way as to form two regions of enhanced spectral reflectance (D.T. Georgi).

Useful geological information can be obtained only in narrow strips at the passage from bright to dark where the exposure falls on the ramp in the characteristic curve of the film. The instant film used for field recording has limited contrast range, so the effect of shading is severe loss of information.

The strips are rectilinear above 4500 ft depth, but the pattern degenerates to a spiral below that depth (Figure 9). One explanation is that the wellbore is shaped as a quadric cylinder above 4500 ft but is rifled below that depth. Other explanations are failure of the centralizers or the magnetometer below 4500 ft.

J. Geometric Distortions

1. Affine Distortions. Scanner imagery, in contrast to photographic or RBV imagery, has distortions that are due to changes in tracking direction through a frame. Rotation of the scanner axis is a smaller problem for the televiewer, but accelerations in the tracking direction produce nonlinear effects that are uncorrectable so long as the accelerations are unknown. The projective distortions of satellite imagery (Gosh 1972; Colvocoresses and McEwen 1973; Kratky 1974; and Wong 1975) have a counterpart in televiewer imagery that is due to off-centering of the tool in an elliptical borehole.

2. Oscillation Patterns. A pattern of fine striations appears on GT-2 imagery. This pattern runs near-vertical, that is, inclined from 0° to 15° with the along-track direction. Along each scan line, the pattern is formed by alternation of bright and dark pixels. Examples are shown in Figures 3 and 8. Grain effect is striping at an angle to the scan lines that is coherent across a minute or more of recording time, as shown in Figure 6. The cause is unknown in satellite RBV imagery, according to Clark (1981).

The striations were originally thought to be caused by scratches on the side of the wellbore. However, they were found, during logging of EE-3A, to grade into the grain effect. Comparing imagery with chart records of the load on the cable allowed us to identify mechanical oscillations as the cause of grain effect. The transducer rotates horizontally in the tool at a rate of about 3 Hz, and at the same time the tool oscillates vertically at a comparable rate. When the ratio of the two frequencies is a whole number, an upward excursion on one scan line is adjacent to an upward excursion on the next scan line. The two excursions are then in phase, and the result looks like a striation running perpendicular to the scan lines. The angle departs from 90° as the ratio of the two frequencies departs from a whole number. The pattern is, therefore, formed by a mechanism that resembles the Lissajous effect. A predominant factor in the frequency of tool oscillation is the length of the logging cable. In images obtained from shallow depth with short cables, the features are fine striae as in GT-2. In images obtained from greater depth with longer cables, the features are a coarse grain effect as in EE-3A.

K. Other Image Artifacts

Televiewer imagery has recording artifacts in common with RBV imagery (Clark 1981). These include repetition and omission of scan lines and line dropouts between frames, as shown in Figure 6. Repetition of scan lines is

due to recording while the tool is stationary. Omission of alternate scan lines in some frames may be due to trigger failures. Omission of scan lines between frames is due to manual film changing. The white (additive) noise level is high, increases downhole, and is probably thermally induced electronic noise. The most important effect is harmonic shading attributed to hole ellipticity or tool off-centering. This degenerates to a spiral below 4500 ft, possibly due to thermal failure of mechanical centralizers.

Televiewer imagery has geometric distortions in common with MSSs on satellite or aircraft platforms. These distortions include oscillation patterns such as striae, striping, and grain effect due to longitudinal oscillations of the tool. Geometric errors that are important in aircraft systems, such as misalignments of the CRT display and the recording camera, nonperpendicular arrangement of the rotation axis of the scanner to the instantaneous field of view, and inaccuracies in centering and alignment of the scanner (Masry and Gibbon 1973), are insignificant for the televiewer.

L. Overall Image Quality

Compared with the results obtained from satellite scanners using modern digital recording and playback systems, the quality of GT-2 televiewer imagery is grossly inferior. Due to severe harmonic shading, less than 5% of the record is in usable contrast range. The images had not been analyzed previously on that account, but they were preserved against the possibility of a feature extraction system being developed. The task is possible, although difficult, using methods described here, where the harmonic shading is rectilinear, as in Figure 8. Where there is a spiral shading pattern, as in Figure 9, the task is extremely difficult and will require a more elaborate interpretation method. These investigations have determined the nature of the advanced interpretation methods that are required. Because of the many simultaneous factors involved, the method will postulate a hole shape, tool location, sonic velocity and type, location, and orientation of natural features on the wellbore surface. The postulations will be verified by comparing a simulation of their effect on the image with the effects observed on the image. The implication is that the process of image formation is too complex to be directly inverted except in the special case of a centered, vertical tool in a circular, vertical wellbore.

V. FEATURE EXTRACTION

A. General Description

In modern digital systems, the raw imagery is processed to remove artifacts and increase the signal-to-noise ratio by scan-line equalization, density smoothing, contrast enhancement, and other procedures that utilize redundant information. Feature extraction is then performed digitally using various pattern-recognition algorithms. However, in this case digital imagery was not available, so manual methods were used.

The feature-extraction method comprised human perception of features, manual annotation, digitization of the annotations using a pencil-type line follower, and acceptance or rejection of each annotation depending upon a simple pattern-recognition procedure. The method was applied interactively with a desktop microcomputer.

B. Flowsheet

The feature extraction subsystem is illustrated in Figure 11. This flowpath is designed for interactive operation, keyed by interrupts. There is, therefore, no prescribed order of program execution. The following is typical.

1. Registration. (1) Find the top and bottom coordinates of the image, in depth downhole, measured along the drill string. (2) Interrogate the wellbore survey to find the nearest two survey points that bracket the image. For these two, carry forward the depths downhole, absolute locations, and absolute orientations of the wellbore axis. (3) Digitize the four fiducial marks of the image and find the registration matrix, M.

2. Feature Extraction. (4) Select a structural trace. (5) Digitize L points on the trace (L is generally between 10 and 30) and convert to coordinates (depth downhole, magnetic azimuth) by premultiplication by M. (6) Determine Fourier coefficients of the trace. Compare the fitted function with actual measurements to determine goodness of fit. If the goodness of fit is too large, reject the trace, record the statistics of the rejected trace, and return to step (4); otherwise, continue. (7) Record the statistics of the accepted trace and carry forward the Fourier coefficients.

3. Location. (8) Using the constant Fourier term from (7) and depths downhole and absolute locations of the nearest survey points from (2), interpolate to find the depth downhole and absolute location of the trace.

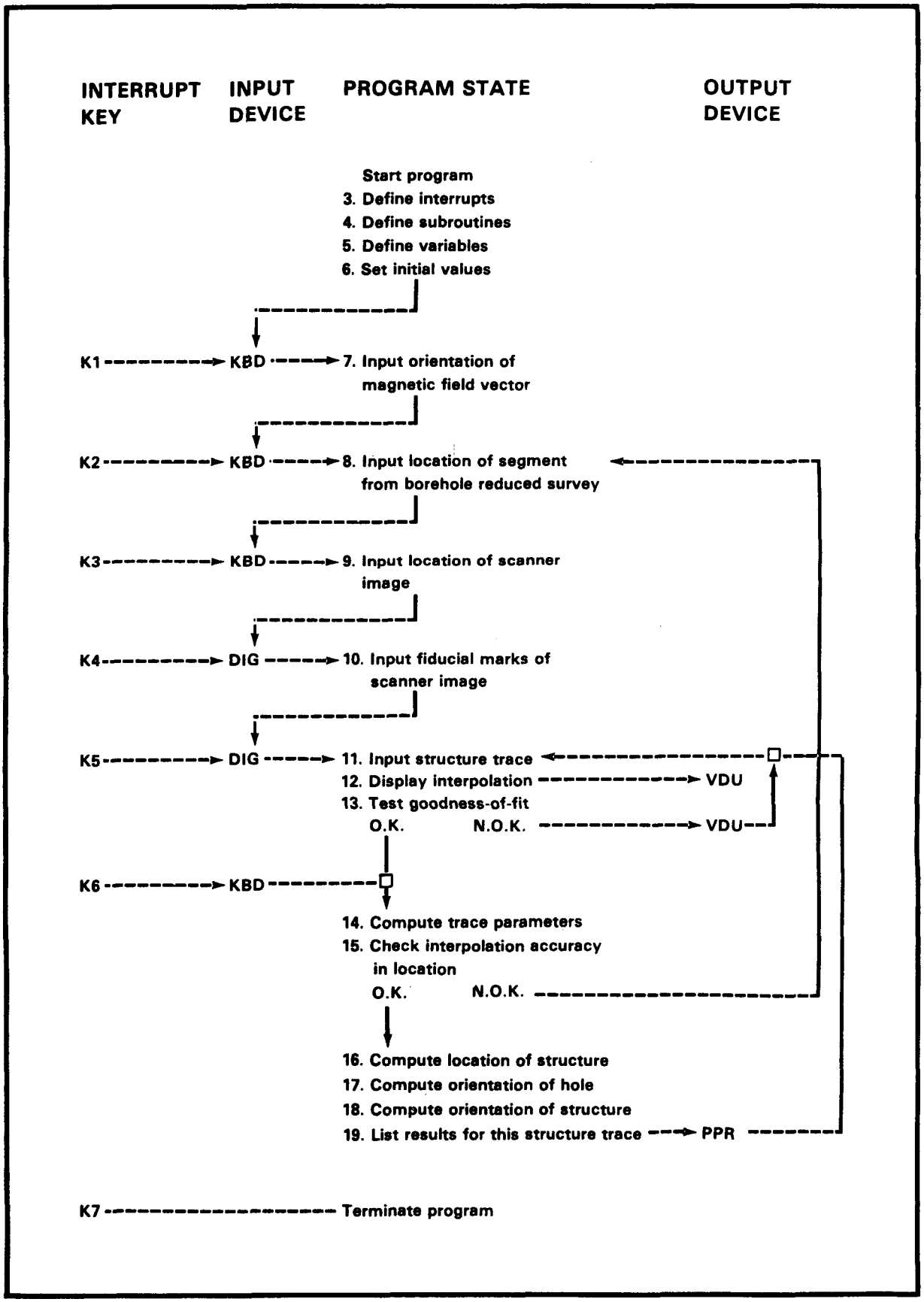

Figure 11. Feature extraction procedure: schematic flowsheet.

4. Orientation. (9) Using depth of the structure from (8) and depths and absolute orientations of the nearest survey points from (2), interpolate to find the orientation of the drill hole at the trace. (10) Using the Fourier phase and amplitude of the trace from (7), average hole diameter from a caliper log for this depth and drill hole orientation from (9), find the absolute orientation of the structure.

5. Continuation. (11) If all traces on the image are not processed, return to step (4). (12) If all images are not processed, return to step (1).

C. Image Registration

Where réseau marks are spaced across a scanner image, as in RBV imagery, position on a scanner image may be determined by nonlinear "mapping polynomials" such as those described by Bernstein and Silverman (1971) and by Masry and Gibbon (1973). There are no réseau marks on televiewer imagery, so we use as registration points a set of n points chosen at the beginning and end of scan lines on a frame. Let x be the azimuth in degrees east of magnetic north and y be the depth downhole in feet. The ith point on the image is assigned to a homogeneous column vector of the form $\underline{z}_i = [x_i, y_i, 1]'$, where ' denotes transpose. The registration points can then be arranged as columns of the 3 x n matrix Z, where

$$Z = \begin{vmatrix} x_1 & x_2 & x_3 & x_4 & \cdots & x_n \\ y_1 & y_2 & y_3 & y_4 & \cdots & y_n \\ 1 & 1 & 1 & 1 & \cdots & 1 \end{vmatrix} .$$

For example, if the two ends of the first and last scan lines are used, n = 4 and

$$Z = \begin{vmatrix} 0 & 360 & 0 & 360 \\ y_1 & y_1 & y_2 & y_2 \\ 1 & 1 & 1 & 1 \end{vmatrix} ,$$

where y_1 is the depth of the first scan line on the frame and y_2 is the depth of the last scan line, in feet. Corresponding to the n fiducial points, let $\underline{c}_1 = [a_1, b_1, 1]'$ be the homogeneous coordinates of the same points as measured with a chart digitizer. These can be arranged columnwise in a matrix C. If M is then the registration matrix, or transformation from chart coordinates to image coordinates, and "*" denotes row-column matrix multiplication, then

$$Z = M*C \quad .$$

To register the image is to find the projective transformation M. One very simple method is to use three registration points, such as the beginning of the first scan line and the beginning and end of the last scan line in the frame. Then n = 3, C and Z are square, and an estimate $\hat{M}$ of M is

$$\hat{M} = C^{-1}*Z \quad . \tag{2}$$

For other values of n, C and Z are not square and the maximum-likelihood estimator of M is the minimum-norm least-squares estimator $\hat{M}$, where

$$\hat{M} = [C'*C]^{-1}*[C'*Z] \quad . \tag{3}$$

In this Equation, $^{-1}$ denotes the 1-inverse (Rao and Mitra 1971, p. 50; Noble 1976).

Numerical errors can be reduced by translating to the mean and scaling to the variance before inversion (the so-called Z-transform). The registration matrix found by these methods is a linear projectivity containing a similarity (scale change), rotation and translation (rigid motion), affine transformation (linear distortion), and projectivity (Gans 1969, p. 177). The projectivity

is the bottom row of $\hat{M}$, and it should be negligible for an instrument functioning properly; that is, the bottom row of $\hat{M}$ should be near [0, 0, 1]. The transformation from chart digitizer coordinates $\underline{c}$ to wellbore coordinates $\underline{z}$ is then given by $\underline{z} = M*\underline{c}$. This is a projective transformation in homogeneous coordinates so that, converting to real space and nonhomogeneous coordinates, the resulting azimuth is $\hat{z}_1/\hat{z}_3$ degrees east of north, and the resulting depth is $\hat{z}_2/\hat{z}_3$ ft downhole.

D. Annotation Method

Annotation was done on Xerox copies in order to preserve the original Polaroid prints. Structures were of two types, discrete and diffuse. Discrete structures appeared on the image as a connected linear trace of low reflectivity. Annotation consisted of detecting and marking the trace as a single line (Figure 12a).

Diffuse structures appeared on imagery as fields of fine, parallel bright fringes or lines. Annotation consisted of fitting a vector trend (Agterberg 1974, p. 494) or streamline, to which the fringes were tangential (Figure 12b). In the latter method the operator guessed a streamline and digitized it, and then the computer drew a best-fit curve to it. If the computer rejected the curve, the operator used the last computer-drawn curve as a guide to improving the streamline. If, after several attempts, the computer still rejected the streamline, the attempt to fit one was abandoned. The computer rejected 46% of all attempts. The rate of annotation varied between 160 and 320 ft (depth downhole) per day, with the higher rate difficult to sustain.

E. Structural Trace in Image Coordinates

The orientation of a plane discrete structure is defined by the orientation vector p, which points normal to the plane, positive down (Figure 13). The orientation of the drill hole is defined by the vector $\underline{h}$, which points down the axis of the hole. The trace of the structure on the wall of a circular drill hole is an ellipse in the plane $\underline{p}$ (Goodman 1976, p. 143) with axes $\underline{s} = \underline{h} \times \underline{p}$ and $\underline{t} = \underline{p} \times \underline{s}$, where x denotes the vector crossproduct. The rotary televiewer describes scan lines normal to $\underline{h}$ with a reference at the point where each scan line crosses the magnetic meridian. In the resultant image (Figure 14) the lines y = constant are scan lines, and the points x = 0 in each scan line are the meridian crossing points. The lines x = constant are generators that run parallel to the axis of the borehole.

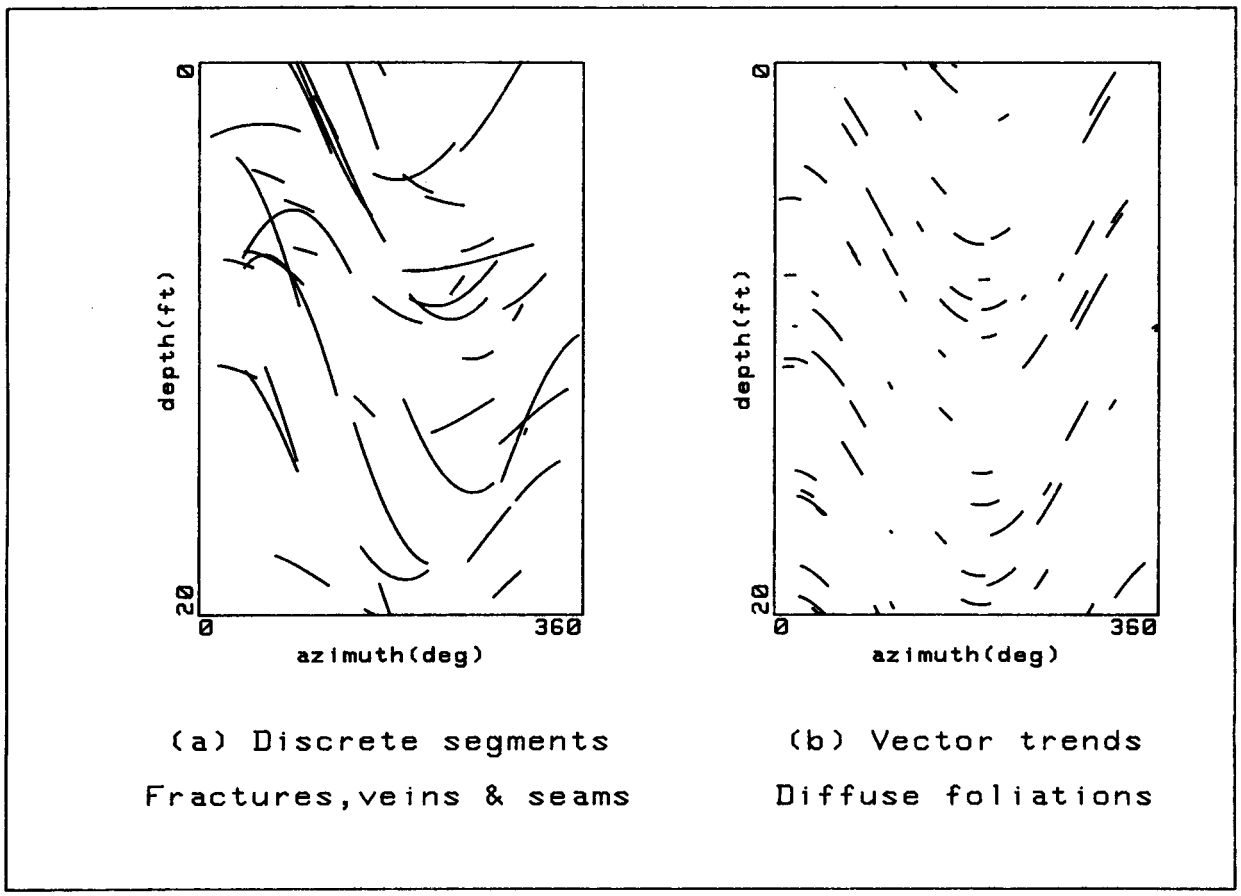

Figure 12. Schematic appearance of (a) discrete elements and (b) diffuse foliation on televiewer imagery.

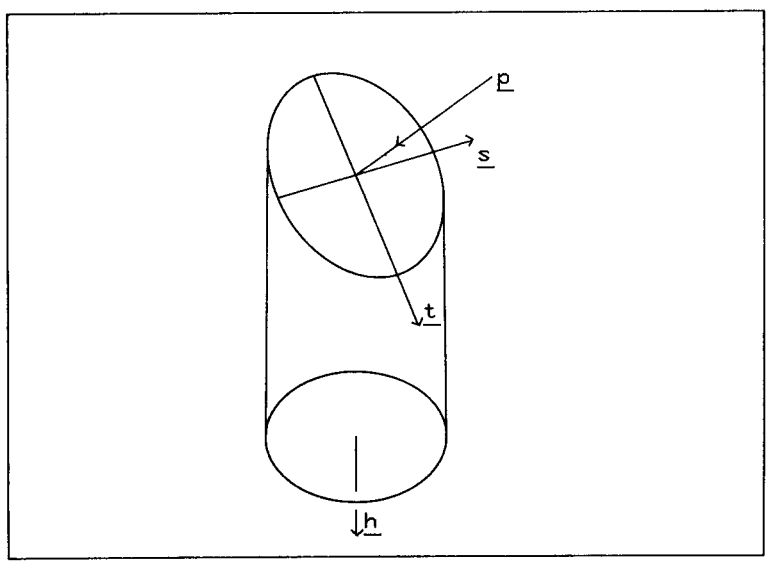

Figure 13. Perspective view of a structure intersecting a wellbore. Two direction vectors are $\underline{p}$, normal to the structure, and $\underline{h}$, the axis of the borehole. The intersection of planes normal to $\underline{p}$ and $\underline{h}$ is a space curve. For a plane structure, centered televiewer, and circular wellbore, the space curve reduces to an ellipse with semiaxes $\underline{s}$ and $\underline{t}$, where $\underline{s} = \underline{h} \times \underline{p}$, $\underline{t} = \underline{p} \times \underline{s}$.

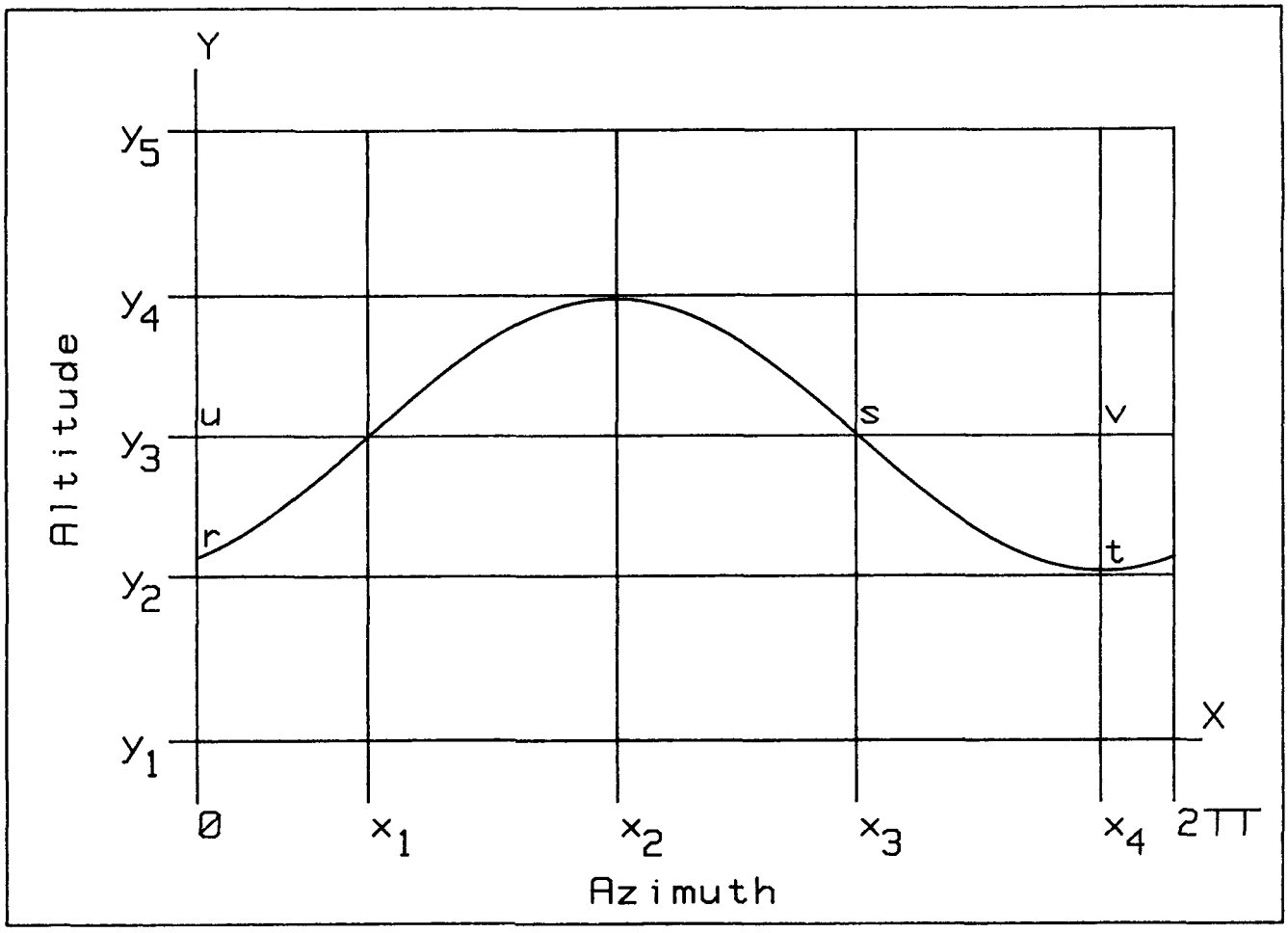

Figure 14. Appearance of a structural trace on a televiewer image. This is the projection of the ellipse curve onto the sensor. Scan lines are y = constant, $0 \leq x \leq 360°$. Generators of the wellbore are x = constant, $0 \leq y$. The locus of the magnetic meridian on the scan lines is the scan-line trigger, x = 0. The projection of the right-handed strike direction is (x_3,y_3). The projection of the dip direction is (x_4y_2). Points s and t are projections of orientations shown in Figure 4.

A plane discrete structure appears on the televiewer image as a harmonic trace. The projection (from Figure 13 to Figure 14) is given by the following:

(1) t, the altitude, corresponds to $[x_4,y_2]$;

(2) for a televiewer rotating clockwise, the projection of s on the image is the descending node, corresponding to $[x_3,y_3]$.

F. Analytical Geometry of Structural Trace

Figure 15 is a view in the plane of the scanner of an elliptical borehole with semidiameters a,b centered at g. The long semidiameter is inclined at θ

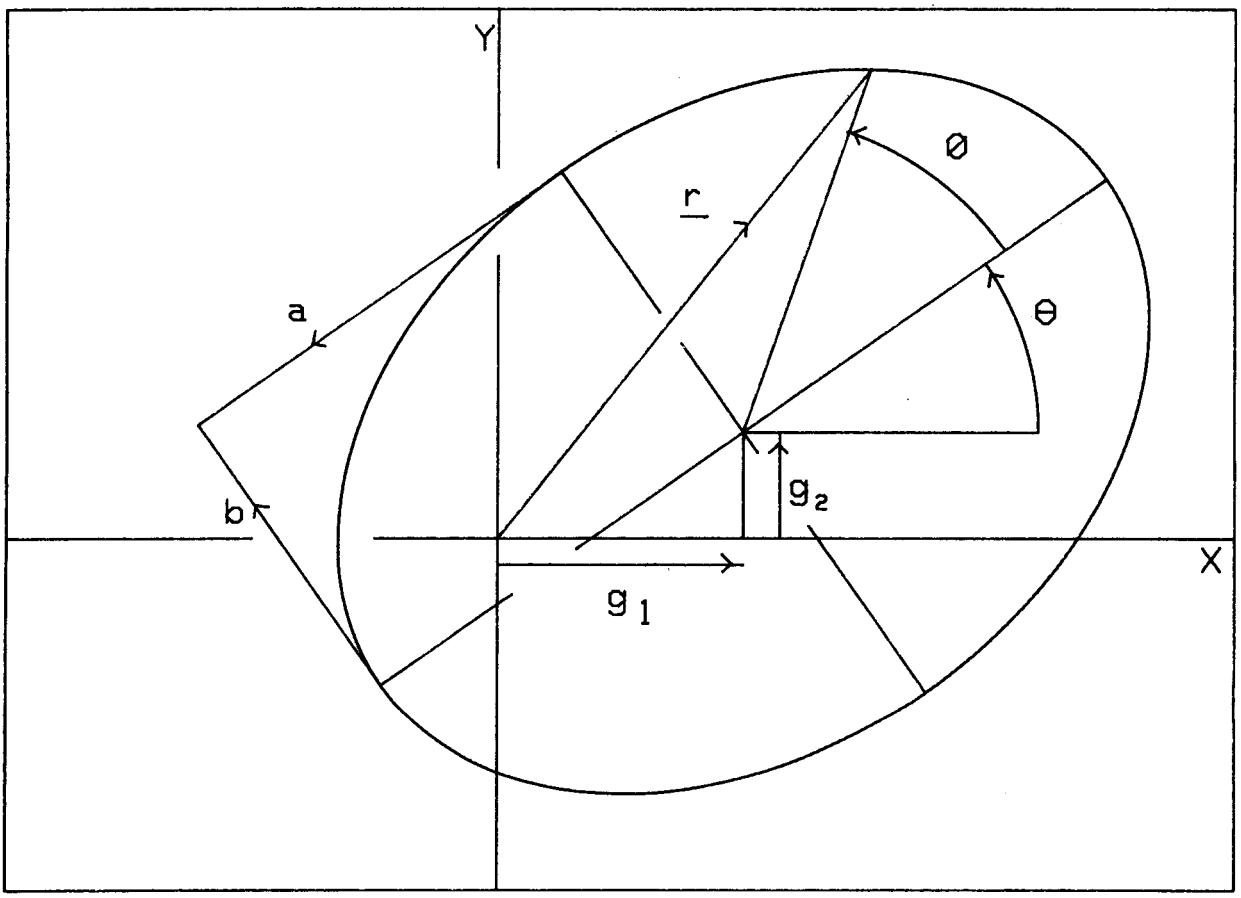

Figure 15. Trace geometry for an elliptical borehole with an off-centered televiewer.

to the X-direction (east). The televiewer is located at (0,0); the center of the borehole at $\underline{g}$. The Y-direction (north) is triggered by the magnetometer. The radius vector $\underline{r}$ to the surface of the borehole is

$$\underline{r} = \underline{g} + \begin{vmatrix} \cos\theta & -\sin\theta & 0 \\ \sin\theta & \cos\theta & 0 \\ 0 & 0 & 1 \end{vmatrix} \begin{vmatrix} a\cos\phi \\ b\sin\phi \\ 0 \end{vmatrix} . \qquad (4)$$

The position vector $\underline{p}$ to a plane through $\underline{q}$ with normal $\underline{n}$ is given by $(\underline{p}-\underline{q})'\underline{n} = 0$. The intersection of the structural plane and the wall of the borehole is $\underline{r} = \underline{p}$ or

$$(\underline{r} - \underline{q})'\underline{n} = 0 \quad . \tag{5}$$

We now assume that the borehole is a right circular cylinder with zero ellipticity and that the televiewer is centered. Set $q = [0,0,y_o]$, $a = b$, $\theta = 0$. Then Equations (4) and (5) yield the trace in Figure 14, where y is the altitude, as

$$y = y_o + (-an_1/n_3) \cos \phi + (-an_2/n_3) \sin \phi \quad . \tag{6}$$

This Fourier series may be written

$$y = C + A \cos \phi + B \sin \phi \quad . \tag{7}$$

Simulations using Equations (4) and (5) produced trace shapes such as are found on the imagery so that the assumptions in the derivation of Equation (6) do not generally apply. However, because of off-centering and ellipticity, the parameters in Equation (2) cannot be reliably estimated if the structures are nonplane, so the traces were fitted by Equation (6).

G. Estimation of Coefficients

For a discrete series of observations, $[x_i,y_i;\ i = 1,2,\ldots L]$, the Fourier coefficients C, A, and B in Equation (7) are found (Davis 1973, p. 265) as the solution to the set of linear Equations:

$$\begin{vmatrix} L & S\{\cos x_i\} & S\{\sin x_i\} \\ S\{\cos x_i\} & S\{\cos x_i \cos x_i\} & S\{\cos x_i \sin x_i\} \\ S\{\sin x_i\} & S\{\sin x_i \cos x_i\} & S\{\sin x_i \sin x_i\} \end{vmatrix} * \begin{vmatrix} C \\ A \\ B \end{vmatrix} = \begin{vmatrix} S\{y_i\} \\ S\{y_i \cos x_i\} \\ S\{y_i \sin x_i\} \end{vmatrix} ,$$

where S{} is summation over i from 1 to L. This may be solved by the minimum-norm least-squares method described previously.

H. Pattern Discrimination

If $e_1, e_2, \ldots, e_f$ are independent and identically distributed random variables, each following a Normal distribution with zero mean and unit variance, then $X^2 = e_1^2 + e_2^2 + e_3^2 \ldots + e_f^2$ follows a chi-square distribution with f degrees of freedom. If we let the e_i be the differences in depth between points observed on the actual trace and the corresponding points on the best-fit trace and assume that these errors are Normally distributed, then X^2 can be used to test the probability of a good fit.

For a centered televiewer in a circular hole, the chi-square statistic for a structural trace is X^2:

$$X^2 = S_{\{}(y_i - C - A \cos x_i - B \sin x_i)^2/(C + A \cos x_i + B \sin x_i)\} \quad , (9)$$

where $S_{\{\}}$ is summation over i from 1 to L. The chi-square test is then applied as follows (Maisel 1971, p. 137; Parratt 1961, p. 184):

(1) Estimate X^2 according to Equation (9).
(2) Set f = L - 3 (three Fourier coefficients estimated).
(3) Set q = 0.05 (95% probability).
(4) Find u = invchi(q): this is the value of X^2 that is exceeded with probability q for f degrees of freedom.
(5) If $X^2 > u$, reject the trace.
    If $X^2 \leq u$, accept the trace.

An algorithm for evaluating invchi is given in the following section. Examples of structural traces found by these methods are illustrated in Figure 16. These are computer reconstructions of traces that passed the pattern discriminator.

I. Numerical Estimation of Invchi

The chi-square probability density function is c(x;f), where x is location on the positive real line, $0 < x$, and f is the (integral) number of degrees of freedom, $0 < f$. The density (Zelen and Severo 1964) is

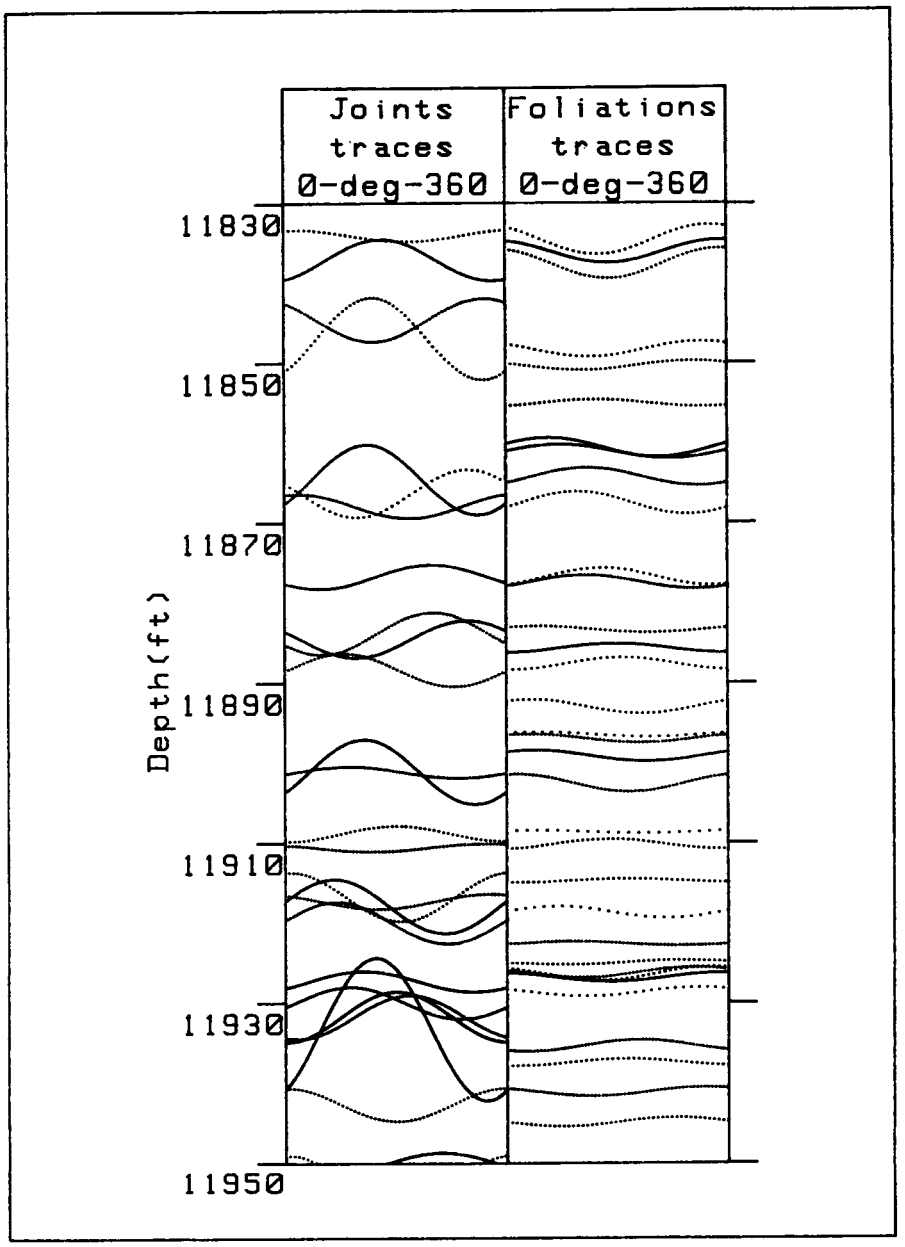

Figure 16. Televiewer logs for EE-3A showing structural traces.

$$c(x;f) = (2G(f/2))^{-1} (x/2)^{(g/2)-1} \exp^{-x/2} .$$

The chi-square cumulative or frequency function is C(u;f), where

$$C(u;f) = S\{c(x;f)\}dx = I(f/2,q/2)/G(f/2) . \quad (10)$$

The term S{}dx is integration over x from 0 to u; I is the incomplete gamma function (Tricomi 1953); and G is the elementary gamma function.

Where q is a given probability, the frequency function in Equation (10) is q = C(u;f). This may be regarded as an operation C on u to give q; thus q = C[u]. The inverse operation is $u = C^{-1}[q]$. The inverse may be found by taking advantage of the fact that C(u;f) tends to a Normal distribution as f tends to infinity. Specifically, for f > 30 (Bury 1975, p. 248),

$$C(u;f) \dashrightarrow N[(x/f)^{1/3};\ 1-2/(9f),\ (2/(9f))^{1/2}] .$$

That is, the variable $(x/f)^{1/3}$ is asymptotically Normal with mean 1-2/(9f) and standard deviation $(2/(9f))^{1/2}$. Thus, given q, we define the inverse function u = invchi(q) as

(1) v = inverf(1 - q), where v is location in the standard Normal distribution;

(2) $u = f[1 - 2/(9f) + v(2/(9f))^{1/2}]^3$, where u is the corresponding location in the chi-square distribution (Zelen and Severo 1964, p. 941).

Computational algorithms for invchi and inverf are listed below.

Algorithm 1: invchi

```
      input:              frequency  q
                  degrees of freedom  f
     return:               location  u

step 1) find Normal location:
        call inverf(1-q, x)
step 2) transform to chi-square asymptotic:
            t1  =  2/(9*f)
            t2  =  x*t1^0.5
            u   =  f*(1-t1+t2)^3
step 3) the procedure is complete.
        the return is u.
```

Algorithm 2: inverf

```
      input: frequency q
     return: location x
```

```
step 1) set coefficients:
              p3  =   1.E-24
              q3  =  -1
              c0  =   2.515517
              c1  =   0.802853
              c2  =   0.010328
              d1  =   1.432788
              d2  =   0.189269
              d3  =   0.001308
step 3) find ranges:
       (a)    q2  =   q
           if q2  ≤  0.5,  go to step (3b)
              q2  =   1 - q
              q3  =   1
       (b) if q2  >   p3,  go to step (4)
              q2  =   p3
step 4) evaluation:
              t   =   ln(1/(q2*q2))
              t   =   t^0.5
              t1  =   c0 + c1*t + c2*t^2
              t2  =   d1*t + d2*t^2 + d3*t^3
              x   =   t - t1/(1 + t2)
              x   =   q3*x
step 5) the procedure is complete.
        the return is x.
```

J. Quality Control

The accuracy and reliability of features estimated by this procedure are described in Part 3 of this report.

K. Prospects for Automatic Feature Extraction

Human detection followed by a pattern discriminator based on a chi-square test for a harmonic trace is possible, as demonstrated by this report, but is not practicable on a sustained basis. A sustained method needs to be automatic. The textures are sufficiently different from each other for automatic methods of feature extraction to be possible. Calculation of physical parameters of the objects appears possible if the televiewer is run simultaneously in intensity mode and caliper mode and is experimentally calibrated against objects of interest.

The pattern discriminator of Section V.H. did not appear to be consistent for the foliations. This is because foliations are nondiscrete elements and the observer, in discretizing them, is fitting a vector trend through a field of tangents (Agterberg 1974, p. 494), so a test for a continuous linear trace does not match the types of errors likely to be generated. While this method

is probably satisfactory for fractures, different pattern-recognition procedures will be required for automatic extraction of foliations.

Because of the many simultaneous factors involved in the formation of a televiewer image, the image is too complex to be directly inverted except in the special case of a centered, vertical tool in a circular, vertical wellbore. Interpretation of the imagery is not simply a matter of writing an electronic scanner record to film and then identifying features by simple visual inspection of the image. It is necessary to model the imaging features and compare the model with the actual image in order to obtain a positive identification of natural features or artifacts. Factors to take into account are hole shape, tool location in the hole, transducer characteristics, sonic velocity in wellbore fluid, and wellbore surface roughness as well as the type, location, and orientation of natural features on the wellbore surface. Effects to be considered include harmonic shading, mechanical oscillations, and a host of effects such as absorption, reflection, and diffraction for specified natural objects.

VI. CONCLUSIONS

A. Image Quality

The televiewer imagery of GT-2 is of grossly inferior quality. Due to severe harmonic shading, less than 5% of the record is in usable contrast range. Digital recording and playback are essential in order to produce images of sufficient quality for satisfactory feature extraction.

B. Feature Extraction

Artifacts are features on the imagery that do not correspond to physically real objects on the wellbore. Artifacts recorded on televiewer imagery are similar to those found on RBV, MSS, and other electronic systems and include repetition and omission of scan lines within frames and dropouts between frames. Recording noise is white (additive) noise on the imagery that increases downhole and is probably thermally induced electronic noise.

Geometric artifacts are features on the imagery due to changes in tracking direction through a frame. The transformation between the scanning spot on the ground and the image-writing spot on the image is not a simple similarity transformation. Televiewer imagery has geometric distortions in common with RBV imagery and with MSSs on satellite or aircraft platforms. Linear

transformations that are important in aircraft systems, such as misalignments of the CRT and recording camera, nonperpendicular arrangement of the rotation axis of the scanner to the instantaneous field of view, and inaccuracies in centering and alignment of the scanner, are not important for the televiewer. However, nonlinear transformations, such as those causing oscillation patterns, are important to feature recognition. Oscillation patterns consist of striae and grain effect. Grain effect is a coarse, discontinuous streakiness, running at an oblique angle to the wellbore axis, that is almost certainly due to tool oscillations. The slope of the streaks on the image is a function of the ratio between the frequency of transducer rotation and the frequency of longitudinal oscillation of the tool suspension assembly. A similar artifact occurs on satellite RBV imagery, cause unknown, but in view of televiewer observations, the cause may be spacecraft vibrations. The fine striae run near-vertical, that is, close to the along-track direction. They first appeared to be abrasion scratches on the wellbore, but in imagery from EE-3A, they appear to grade into grain effect, so they may have a similar cause. Their azimuth varies with depth as piecewise-damped sinusoidal and exponential functions, suggesting a relation to damped longitudinal oscillations of the tool.

Harmonic shading is a tonal gradation that divides the image into alternating over- and underexposed vertical strips. Film density varies across-track as a harmonic function of azimuth. The simplest case is where density varies as COS(2*Azimuth). Mechanisms that have been considered included path attenuation and system aberrations, but the effect can be explained as due to specular reflection following Snell's Law in a misaligned mirror. The effect is then due to an off-centered tool in an elliptical (noncircular) wellbore. It degenerates to a spiral below 4500 ft, either due to off-centering, possibly resulting from thermal failure of mechanical centralizers, or due to change of hole shape from a quadric to a rifled cylinder.

Natural features on the imagery include geological structures and other physically real objects on the surface of the wellbore such as vughs, chips, and breakouts. Geological structures include induced fractures, natural joints, faults, cleavages, foliations, and bedding.

Fractures and joints are usually open to the wellbore with apertures ranging from hairline cracks to several-millimeters-wide cracks. The characteristic texture is a dark, discrete linear feature: a finite connected object with connectivity of one. Fractures are visible at a fraction of the

IFOV, a dimension that is substantially below NASA's theoretical limit. The reason for this anomalous result is probably razor-blade or wave-guide absorption.

Foliation in gneiss comprises discrete foliations such as grains, folia, and bands, with mean spacings of 3, 10, and 30 mm, respectively, as well as diffuse foliations such as preferred orientation of grains or grain boundaries.

Discrete foliations are detected because the coefficient of reflectance varies between adjacent folia. The most important parameter is probably bulk modulus: representative ratios are feldspar: mica: quartz = 1.55:1.18:1, making foliation a low-contrast target on television criteria. Thick mineral bands are expressed as regions of different first- and second-order textural statistics. Thin mineral bands are expressed on the imagery as strips of different density. The image features correspond to real objects and the IFOV grid acts as simply a low-pass filter.

Diffuse foliations are fields of elongated grains, with a ratio of spatial frequencies in two perpendicular directions of about 0.3:0.2 mm^{-1}. We have detected foliation on imagery from GT-2 and EE-3A from the USGS intensity-mode imagery. However, it has not been detected on intensity-mode imagery made with other instruments.

The textural statistics of the diffuse texture have not been quantified. They have been described as a pattern of parallel bright linears of high spatial frequency and also as an eigenfeature. The causes of this texture are unknown. Possibilities include spurious resolution, edge diffraction, and a phase grating.

Not knowing the specific mechanisms responsible for the diffuse texture, we cannot know whether the correspondence between geological objects on the wellbore and textural features on the image is one-to-one or many-to-one, that is, whether the features are real objects or rainbows.

Breakouts in GT-2 are small triangular wedges at intervals along the trace of fractures and thin, dark micaceous seams. These may be chips or chattermark due to tool abrasion or incipient breakouts due to stress corrosion.

C. Automatic Feature Extraction

Because of the many simultaneous factors involved in the formation of a televiewer image, advanced interpretation methods are required. A conclusion

of this study is that the process of image formation is too complex to be directly inverted except in the special case of a centered, vertical tool in a circular, vertical wellbore. In other cases the imagery is not comprehensible; that is, many features cannot be positively identified because a large number of contributory factors may be involved. Interpretation of televiewer imagery is not simply a matter of writing an electronic scanner record to film and then identifying features by simple visual inspection of the image. Instead, it is necessary to construct a model or numerical simulation of the imaging process. This conclusion is in accord with current trends in borehole geophysics research and with Georgi's research.

This investigation shows that components of such an "imaging model" include hole shape, tool location in the hole, transducer characteristics, and sonic velocity in wellbore fluid as well as the type, location, and orientation of natural features on the wellbore surface. Effects to be included in the model include harmonic shading, mechanical oscillations, and a host of effects such as absorption, reflection, and diffraction for specified natural objects.

The postulates of such a model would be the type, attitude, and parameters of natural objects on the wellbore surface. The postulates would be verified by comparing an image constructed from the postulates with the actual image as observed.

REFERENCES

Aamodt, R.L., 1974, "Experimental Measurement of In Situ Stress in Granite by Hydraulic Fracturing," Los Alamos Scientific Laboratory report LA-5605-MS.

Aamodt, R.L., 1977, "Hydraulic Fracture Experiments in GT-1 and GT-2," Los Alamos Scientific Laboratory report LA-6712.

Agterberg, F.P., 1974, Geomathematics. Mathematical Background and Geoscience Applications (Elsevier, Amsterdam).

Albright, J.N., 1975, "Temperature Measurements in the Precambrian Section of Geothermal Test Hole No. 2," Los Alamos Scientific Laboratory report LA-6022-MS.

Bachofer, B.T., 1973, "ERTS-1 Data Product Performance," Symp. on Significant Results Obtained from ERTS-1, v. 1, section A, pp. 1-9, NASA, Greenbelt.

Bernstein, R., and H. Siverman, 1971, "Digital Techniques for Earth Resource Image Data Processing," Tech. Rep., n. FSC 71-6017, I.B.M., Gaithersburg.

Briggs, R.O., 1964, "Development of a Downhole Television Camera," Fifth Annual SPWLA Logging Symposium, Midland, Texas, May 13-15, 1964.

Brookins, D.G., R.B. Forbes, D.L. Turner, A.W. Laughlin, and C.W. Naeser, 1977, "Rb-Sr, K-Ar, and Fission-Track Geochronological Studies of Samples from LASL Drill Holes GT-1, GT-2, and EE-1," Los Alamos Scientific Laboratory report LA-6829-MS.

Brookins, D.G., and A.W. Laughlin, 1983, "Rb-Sr Geochronological Investigations of Precambrian Samples from Drill Holes GT-1, GT-2, EE-1, and EE-2. Los Alamos Hot Dry Rock program, Fenton Hill, New Mexico," J. Volcanol. Geotherm. Res., v. 15, pp. 43-58.

Bury, K.V., 1975, Statistical Models in Applied Science (Wiley, New York).

Campbell, C.E., 1962, "The Optimization of Photographic Systems," Photogramm. Eng., v. 38, n. 1, pp. 33-35.

Caunt, G.W., 1914, Infinitesimal Calculus (Oxford).

Clark, W.P., 1981, "Landsat 3 Return Beam Vidicon Response Artifacts. A Report on RBV Photographic Product Characteristics and Quality Coding System," EROS Data Center, Sioux Falls, Department of Interior, Washington.

Colvocoresses, A.P., 1972, "Image Resolutions for ERTS, Skylab and Gemini/Apollo," Photogramm. Eng., v. 38, n. 1, pp. 33-35.

Colvocoresses, A.P., and R.B. McEwen, 1973, "Progress in Cartography, EROS program," Symp. on Significant Results Obtained from ERTS-1, NASA, Greenbelt.

Davis, J.C., 1973, Statistics and Data Analysis in Geology (Wiley, New York).

Davis, J.C., and F.W. Preston, 1972, "Optical Processing: An Alternative to Digital Computing," Geol. Soc. Am., Special Paper, n. 146, pp. 49-68.

Delisle, G., 1975, "Determination of Permeability of Granitic Rocks in GT-2 from Hydraulic Fracturing Data," Los Alamos Scientific Laboratory report LA-6169-MS.

Dempsey, J.C., and J.R. Hickey, 1958, "Use of a Borehole Camera for Visual Inspection of Hydraulically-Induced Fractures," Producers Monthly, June 1958, pp. 18-21.

Duntley, S.Q., 1948, "The Visibility of Distant Objects," J. Opt. Soc. Am., v. 38, n. 3, pp. 237-249.

East, J.H., Gardner, E.D., 1964, "Oil-Shale Mining, Rifle, Colo., 1944-56," USBM Bull., n. 611.

Forsythe, W.E., 1954, Smithsonian Physical Tables, 9th edn. (Smithsonian Institution, Washington).

Gans, D., 1969, Transformations and Geometries (Appleton-Century-Crofts, New York).

Georgi, D.T., no date, "Geometrical Aspects of Borehole Televiewer Images," unpublished report, Exxon Production Research, Houston.

Goodman, R.E., 1976, Methods of Geological Engineering in Discontinuous Rocks (West Publishing Co., St. Paul).

Gosh, S.K., 1972, "Deformations of Space Photos," Photogramm. Eng., v. 38, n. 4, pp. 361-366.

Haas, I.S., B.T. Bachofer, and G.P. Fishman, 1972, Key Technological Challenges in the Earth Resoures Technology Satellite Program, L.G. Napolitano, P. Contensou, and W.F. Hilton, editors, Astronautical Research 1972 (D. Reidel Pub. Co., Dordrecht)

Heimlich, R.A., 1976, "Morphology of Zircons from Precambrian Rocks Penetrated by Geothermal Test Hole GT-2," Los Alamos Scientific Laboratory report LA-6433-MS.

Hinz, K., and R. Schepers, 1981, "SABIS--The Digital Version of the Borehole Televiewer," WBK, Institute of Geophysics, Bochum, West Germany.

Hotchkiss, R.N., F.E. Washer, and F.W. Rosberry, 1950, "Spurious Resolution of Photographic Lenses," Proc. Opt. Soc. Am., v. 40, p. 802, abstr.

Hotchkiss, R.N., F.E. Washer, and F.W. Rosberry, 1951, "Spurious Resolution of Photographic Lenses," J. Opt. Soc. Am., v. 41, n. 9, pp. 600-603.

Howell, B.F., 1959, Introduction to Geophysics (McGraw-Hill, New York).

Jensen, O.F., and W. Ray, 1965, "Photographic Evaluation of Water Wells," The Log Analyst, March, pp. 15-26.

Joos, J.G., 1958, Theoretical Physics, 3rd. edn. (Blackie & Son, Glasgow).

Julesz, B., 1975, "Experiments in the Visual Perception of Texture," Sci. Am., v. 232, n. 4, pp. 34-43.

Keller, J.B., 1961, "Geometrical Theory of Diffraction," J. Opt. Soc. Am., v. 52, n. 2, pp. 116-130.

Kintzinger, P.R., and F.G. West, 1976, "Seismic Reconnaissance of the Los Alamos Scientific Laboratory's Hot Dry Rock Geothermal Project Area," Los Alamos Scientific Laboratory report LA-6435-MS.

Kintzinger, P.R., C.B. Reynolds, F.G. West, and G. Suhr, 1978, "Seismic Reflection Surveys near LASL Geothermal Site," Los Alamos Scientific Laboratory report LA-7228-MS.

Kotyakhov, F.I., and S.A. Serbrennikov, 1964, "Evaluation of the Distribution of Fractures in Oil and Gas Reservoirs by Subsurface Photography," Geol. Nefti. i Gaza, pp. 26-30.

Kratky, V., 1974, "Cartographic Accuracy of ERTS", Photogramm. Eng., v. 40, n. 2, pp. 203-212.

Laughlin, A.W., and A.C. Eddy, 1977, "Petrography and Geochemistry of Precambrian Rocks from GT-2 and EE-1," Los Alamos Scientific Laboratory report LA-6930-MS.

Laughlin, A.W., A.C. Eddy, R. Laney, and M.J. Aldrich, 1983, Geology of the Fenton Hill, New Mexico, Hot Dry Rock Site," J. Volcanol. Geotherm. Res., v. 15, pp. 21-41.

Maisel, L., 1971, Probability, Statistics and Random Processes (Simon & Schuster, New York)

Masry, S.E., and J.G. Gibbon, 1973, "Distortion and Rectification of IR," Photogramm. Eng., v. 39, n. 8, pp. 845-849.

McLaren, A.C., R.G. Turner, J.N. Boland, and B.E. Hobbs, 1970, "Dislocation Structure of the Deformation Lamellae in Synthetic Quartz: A Study by Electron and Optical Microscopy," Contr. Mineral. and Petrol., v. 29, pp. 104-115.

Morrone, M.C., J. Ross, D.C. Burr, and R. Owens, 1986, "Mach Bands Are Phase Dependent," Nature Phys. Sci., v. 324, November, pp. 250-253.

Mullins, J.E., 1966, "New Tool Takes Photos in Oil and Mud-Filled Wells," World Oil, June, pp. 91-94.

NASA, 1972, ERTS Data Users Handbook, NASA, Greenbelt.

Noble, B., 1976, "Methods for Computing the Moore-Penrose Generalized Inverse, and Related Matters," M.Z. Nashed, editor, Generalized Inverses and Applications (Academic Press, New York), pp. 245-301.

Parratt, L.G., 1961, Probability and Experimental Errors in Science (Wiley, New York).

Perkins, P.C., 1973, "Petrography of Some Rock Types of the Precambrian Basement near the Los Alamos Scientific Laboratory Geothermal Test Site, Jemez Mountains, New Mexico," Los Alamos Scientific Laboratory report LA-5129.

Pettitt, R.A., 1975a, "Planning, Drilling, and Logging of Geothermal Test Hole GT-2, Phase I," Los Alamos Scientific Laboratory report LA-5819-PR.

Pettitt, R.A., 1975b, "Planning, Drilling, and Logging of Geothermal Test Hole GT-2, Phase II," Los Alamos Scientific Laboratory report LA-5897-PR.

Pettitt, R.A., 1975c, "Testing, Drilling, and Logging of Geothermal Test Hole GT-2, Phase III," Los Alamos Scientific Laboratory report LA-5965-PR.

Plumb, R.A., and S.H. Hickman, 1985, "Stress-Induced Elongation. A Comparison Between the Four-Arm Dipmeter and the Borehole Televiewer in the Auburn Geothermal Well," J. Geophys. Res., v. 90, n. B7, pp. 5513-5521.

Preston, F.W., and J.C. Davis, 1972, "Applications of Optical Processors to Geological Images in Machine Perception of Patterns and Pictures," The Institute of Physics, London, pp. 223-232.

Purtymun, W.D., 1973, "Geology of the Jemez Plateau West of Valles Caldera," Los Alamos Scientific Laboratory report LA-5124-MS.

Purtymun, W.D., F.G. West, and R.A. Pettitt, 1974, "Geology of Geothermal Test Hole GT-2, Fenton Hill Site, July 1974," Los Alamos Scientific Laboratory report LA-5780-MS.

Rao, C.R., and S. Mitra, 1971, Generalized Inverse of Matrices and Its Applications (Wiley, New York).

Rosenberg, P., 1971, "Resolution, Detectability and Recognizability," Photogramm. Eng., v. 37, n. 12, pp. 1255-1258.

Schade, O.H., 1948a, "Electro-optical Characteristics of Television Systems. Part 1 - Characteristics of Vision and Visual Sytems," RCA Rev., v. 9, n. 1, pp. 5-37.

Schade, O.H., 1948b, "Electro-optical Characteristics of Television Systems. Part 2 - Electro-optical Specifications for Television Systems," RCA Rev., v. 9, n. 2, pp. 245-286.

Schade, O.H., 1964, "An Evaluation of Photographic Image Quality and Resolving Power," J. Soc. Motion Pict. Television Engrs., v. 73, n. 2, pp. 81-119.

Sheriff, R.E., and L.P. Geldart, 1982, Exploration Seismology. History, Theory and Data Acquisition, v. 1 (Cambridge University Press).

Sibbitt, W.L., 1976, "Preliminary Measurements of the Thermal Conductivity of Rocks from LASL Geothermal Test Holes GT-1 and GT-2," Los Alamos Scientific Laboratory report LA-6199-MS.

Simmons, G., and A. Eddy, 1976, "Microcracks in GT-2 Cores," EOS, Trans. Am. Geophys. Union, v. 57, p. 353 (abstr).

Slemmons, D.B., 1975, "Fault Activity and Seismicity near the Los Alamos Scientific Laboratory Geothermal Test Site, Jemez Mountains, New Mexico," Los Alamos Scientific Laboratory report LA-5911-MS.

Trice, R., and N. Warren, 1977, "Preliminary Study on the Correlation of Acoustic Velocity and Permeability in Two Granodiorites from the LASL Fenton Hill Deep Borehole GT-2 near the Valles Caldera, New Mexico," Los Alamos Scientific Laboratory report LA-6851-MS.

Tricomi, F.G., 1953, "The Incomplete Gamma Function and Related Functions," in A. Erdelyi, editor, Higher Transcendental Functions (McGraw-Hill, New York), v. 2, pp. 133-152.

Trorey, A.W., 1970, "A Simple Theory for Seismic Diffractions," Geophysics, v. 35, n. 5, pp. 762-784.

Turner, F.J., and L.E. Weiss, 1963, Structural Analysis of Metamorphic Tectonites (McGraw-Hill, New York).

Waters, K.H., 1981, Reflection Seismology. A Tool for Energy Resource Exploration, 2nd edn. (John Wiley & Sons, New York).

Weisskopf, V.F., 1968, "How Light Interacts with Matter," Sci. Am., v. 219, n. 3, pp. 60-82.

Welch, R., 1972, "Quality and Applications of Aerospace Imagery," Photogramm. Eng., v. 38, n. 4, pp. 379-398.

West, F.G., 1974, "Geohydrology of the Jemez Plateau," Los Alamos Scientific Laboratory document LA-UR-74-119.

West, F.G., P.R. Kintzinger, and W.D. Purtymun, 1975a, "Hydrologic Testing Geothermal Test Hole No. 2," Los Alamos Scientific Laboratory report LA-6017-MS.

West, F.G., P.R. Kintzinger, and A.W. Laughlin, 1975b, "Geophysical Logging in Los Alamos Scientific Laboratory Geothermal Test Hole No. 2," Los Alamos Scientific Laboratory report LA-6112-MS.

West, F.G., and A.W. Laughlin, 1976, "Spectral Gamma Logging in Crystalline Basement Rocks," Geology, v. 4, pp. 617-618.

Wong, K.W., 1975, "Geometric and Cartographic Accuracy of ERTS-1 Imagery," Photogramm. Eng., v. 41, n. 5, pp. 621-635.

Zartment, R.E., 1979, "Uranium, Thorium, and Lead Concentrations and Lead Isotopic Composition of Biotite Granodiorite (Sample 9527-2b) from LASL Drill Hole GT-2," Los Alamos Scientific Laboratory report LA-7923-MS.

Zelen, M., and N.C. Severo, 1964, "Probability Functions," in M. Abramowitz and I.A. Stegum, editors, Handbook of Mathematical Functions, National Bureau of Standards, Applied Mathematics Series n. 55, US Department of Commerce (US Government Printing Office, Washington, D.C.), pp. 925-995.

Zemanek, J., 1971, "Beam Behaviour Within the Near Field of a Vibrating Piston," J. Acoust. Soc. Am., v. 49, pt. 1, pp. 181-191.

Zemanek, J., R.I. Caldwell, E.E. Glenn, S.V. Holcomb, L.J. Norton, and A.J.D. Straus, 1969, "The Borehole Televiewer--A New Logging Concept for Fracture Location and Other Types of Borehole Inspection," J. Pet. Tech., v. 21, pp. 762-774.

Zemanek, J., E.E. Glenn, L.J. Norton, and R.L. Caldwell, 1970, "Formation Evaluation by Inspection with the Borehole Televiewer," Geophysics, v. 35, pt. 2, pp. 254-269.